Inspecting the supernova-gamma-ray-burst connection with high-energy neutrinos

Tamborra, I.; Ando, S.

DOI
10.1103/PhysRevD.93.053010

Publication date
2016

Document Version
Final published version

Published in
Physical Review D. Particles and Fields

PHYSICAL REVIEW D 93, 053010 (2016)

Inspecting the supernova–gamma-ray-burst connection with high-energy neutrinos

Irene Tamborra* and Shin'ichiro Ando

GRAPPA Institute, University of Amsterdam, 1098 XH Amsterdam, The Netherlands

(Received 9 December 2015; revised manuscript received 16 February 2016; published 14 March 2016)

Long-duration gamma-ray bursts (GRBs) have been often considered as the natural evolution of some core-collapse supernovae (SNe). While GRBs with relativistic jets emit an electromagnetic signal, GRBs with mildly relativistic jets are opaque to photons and therefore could be detectable through neutrinos only. We discuss the possibility that successful GRBs and mildly relativistic jets belong to the same class of astrophysical transients with different Lorentz factor Γ_b and study the production of high-energy neutrinos as a function of Γ_b, by including both proton-photon and proton-proton interactions. By assuming a SN-GRB connection, we find that the diffuse neutrino emission from optically thick jets with Lorentz factors lower than the ones of successful GRBs can be one of the main components of the observed IceCube high-energy neutrino flux. Moreover, under the assumption that all these jets belong to the same class of astrophysical transients, we show that the IceCube high-energy neutrino data provide indirect constraints on the rate of nonsuccessful jets, favoring a local rate lower than tens of percent of the local SN rate. These limits are currently comparable to dedicated searches on choked sources and are expected to become tighter with the accumulation of more high-energy neutrino data.

DOI: 10.1103/PhysRevD.93.053010

I. INTRODUCTION

Gamma-ray bursts (GRBs) are among the most energetic astrophysical transients [1–3] and possibly sources of ultra-high-energy cosmic rays [4,5]. Several observations point toward a connection between long-duration GRBs and core-collapse supernovae (SNe) [6]. The most likely scenario is that an accretion disk surrounding a black hole forms soon after the core collapse, and a jet originates [7]. Such a hypothesis is supported by the fact that SNe and GRBs are expected to release a comparable amount of kinetic energy.

Once the jet is formed, two extreme scenarios may be foreseen: the jet is either highly or mildly relativistic. The former corresponds to an ordinary long-duration GRB with Lorentz factor Γ_b of $\mathcal{O}(10^2 - 10^3)$, where the emission of high-energy neutrinos is accompanied by an electromagnetic counterpart. The latter stands for a baryon-rich jet with a Lorentz factor of a few, where no electromagnetic counterpart is expected, the jet is optically thick, and only neutrinos are able to escape; in the following, these jets will be dubbed as "baryon-rich or low-Γ_b jets."

The IceCube telescope at the South Pole should be sensitive to any of the above classes of GRBs, given their sizeable neutrino production. However, all the GRB dedicated searches performed from IceCube over the past years reported negative results [8–13], constraining the theoretical models employed to explain the GRB neutrino emission [14–16].

The IceCube experiment recently detected astrophysical neutrinos with the highest energies ever observed [17–22]. The current data set is compatible with an equal distribution of such neutrinos in flavor and an isotropic allocation in the sky. Various astrophysical sources such as starburst galaxies, low-luminosity gamma-ray bursts, and active galactic nuclei have been considered as they might produce a neutrino flux comparable to the detected one [1,23–26]. However, more recent analyses point toward a lower neutrino flux from star-forming galaxies and blazars than previously expected; see, e.g., Refs. [27–29]. Such recent developments leave open the quest on the origin of the IceCube high-energy events and suggest faint or low-luminosity sources as plausible components of the measured flux (see also the discussion in Refs. [30,31]), besides yet unknown astrophysical sources. The diffuse neutrino emission from low-luminosity GRBs [32–35] could indeed partly explain the IceCube PeV events [36–39].

In this paper, we assume that high- and low-Γ_b jets belong to the same GRB family [6,7,40–44] and that the local rate of such jets progressively increases as Γ_b decreases, reflecting the fact that the baryon-rich sources could be more abundant than the ordinary GRBs [45,46]. We expect that PeV neutrinos are mostly produced through proton-photon ($p\gamma$) interactions in jets with high Γ_b, while TeV neutrinos are emitted from baryon-rich sources mostly by means of proton-proton (pp) interactions [45–49]. To estimate the high-energy neutrino emission from astrophysical jets as a function of Γ_b, we model the neutrino emission as generally as possible and by including both pp and $p\gamma$ interactions. We tune the local rate of high-Γ_b bursts

*Present address: Niels Bohr International Academy, Niels Bohr Institute, Blegdamsvej 17, 2100 Copenhagen, Denmark.

to the observed one of high-luminosity GRBs and assume that the one of the low-Γ_b jets is a fraction of the local core-collapse SN rate.

The purpose of our work is to investigate whether IceCube high-energy neutrino data can constrain the SN-GRB connection and possibly allow us to extrapolate upper bounds on the abundance of baryon-rich jets. We also discuss the range where pp and $p\gamma$ interactions dominate the neutrino production as a function of the Lorentz factor Γ_b and find that optically thick jets with Γ_b lower than the one of successful GRBs, e.g., $\Gamma_b \sim \mathcal{O}(10-100)$, could provide a substantial contribution to the observed IceCube flux of high-energy neutrinos.

The paper is organized as follows. In Sec. II, we define the jet emission model and estimate the expected high-energy neutrino production from these sources. In Sec. III, we study the diffuse emission of high-energy neutrinos from astrophysical jets as a function of Γ_b. Bounds on the physics of baryon-rich jets through the IceCube high-energy neutrino data as well as the dependence of our results from the jet model parameters are discussed in Sec. IV. The outlook and conclusions are presented in Sec. V.

II. HIGH-ENERGY NEUTRINO PRODUCTION IN RELATIVISTIC JETS

In this section, we define a generic model for the high-energy neutrino emission from astrophysical relativistic jets by including pp and $p\gamma$ interactions. Besides studying the cooling of protons as a function of Γ_b, we discuss cooling processes of pions, kaons, and muons as well as the expected neutrino fluence.

A. Jet emission properties

Independently from the bulk Lorenz factor Γ_b, we consider a typical jet with total energy $\tilde{E}_j \sim 3\times 10^{51}$ erg,[1] jet opening angle $\theta_j \sim 5$ deg, total duration $\tilde{t}_j \sim 10$ s, and total jet luminosity $\tilde{L}_j = \tilde{E}_j/\tilde{t}_j$ [3]. Internal shocks between the jet plasma ejecta occur at $\tilde{r}_j \sim 2\Gamma_b^2 c t_v/(1+z)$ with $t_v \sim 0.1$ s the jet variability time, c the speed of light, and z the redshift. The isotropic luminosity carried by photons in successful bursts is $\tilde{L}_{\rm iso} = 2(1+z)^2 L_j \epsilon_e/(0.3\theta_j^2)$,[2] with $\epsilon_e = 0.1$ the energy fraction carried by electrons [3,38,50]. In general, one could expect the jet properties to vary as a function of Γ_b. However, we do not have data on baryon-rich jets and assume that their properties are on average comparable to the ones of successful bursts for the sake of simplicity. The similarity between kinetic energies of relativistic GRB jets and nonrelativistic SN explosions may support such an assumption. Nevertheless, we refer the interested reader to Sec. IV for a discussion on the dependence of our results on the adopted model parameters.

To caractherize the typical photon energy, we introduce the Thomson optical depth [48],

$$\tau'_T = \frac{\sigma_T n'_e \tilde{r}_j}{\Gamma_b}, \tag{1}$$

with the comoving electron density similar to the one of baryons,

$$n'_e \simeq n'_p = \frac{L_j(1+z)^4}{m_p c^5 \Gamma_b^6 8\pi\theta_j^2 t_v^2}, \tag{2}$$

where $n'_p = [E_j(1+z)]/(m_p c^2 \Gamma_b V')$, m_p is the proton mass, and $V' = 2\pi\theta_j^2 \Gamma_b \tilde{r}_j^2 c t_j/(1+z)$ is the comoving volume.

The energy associated to the jet magnetic field B is

$$\frac{B'^2}{8\pi} \simeq \frac{2\epsilon_B E'_j(1+z)}{\pi\theta_j^2 \tilde{r}_j^2 c t_j \Gamma_b}, \tag{3}$$

$\epsilon_B \simeq 0.1$ being the fraction of the total energy converted into magnetic energy. Note that we adopt $B'^2/(8\pi) = 4\epsilon_B E'_j/V'$ [3,38]. Previous work on the topic does not always include the constant numerical factor in the definition of the magnetic energy density (see, e.g., Ref. [14]); therefore, care should be taken when comparing our results with the ones reported in part of the existing literature.

In the case of optically thin sources ($\tau'_T < 1$), the photon energy distribution is nonthermal with a typical energy $E'_\gamma = (\hbar\epsilon_e^2 m_p^2 e B')/(m_e^3 c)$ [51], i.e.,

$$E'_{\gamma,\text{non-th}} \simeq \frac{(1+z)\epsilon_{e,-1}^{3/2}\epsilon_{B,-1}^{1/2}\tilde{L}_{\rm iso,52}^{1/6}}{\Gamma_b t_{v,-2}^{2/3}}\ \text{MeV}, \tag{4}$$

with $\epsilon_e \simeq 0.1$ the energy fraction carried by the electrons. The subscripts in the above equation stand for the typical order of magnitude of the quantities defining $E'_{\gamma,\text{non-th}}$, i.e., $\epsilon_{e,-1} = \epsilon_e/0.1$, $\tilde{L}_{\rm iso,52} = \tilde{L}_{\rm iso}/(10^{52}\ \text{erg})$, and similarly for the other variables.

On the other hand, when $\tau'_T \geq 1$, photons thermalize and have an average blackbody temperature [48]:

$$E'_{\gamma,\rm th} \simeq \left(\frac{15\hbar^3 c^2 \epsilon_e E_j}{2\pi^4 \tilde{r}_j^2 t_j}\right)^{1/4}. \tag{5}$$

Therefore, the most general expression for the characteristic photon energy is

[1] For each quantity X, we adopt $\tilde{X}$, X', and X for the physical quantity defined in the source frame, in the jet comoving frame, and in the observer frame, respectively.

[2] As pointed out in Ref. [50], the scaling relation between $\tilde{L}_{\rm iso}$ and L_j is characterized by a large uncertainty that we assume to be fixed to its best-fit value (0.3 ± 0.2); variations within the allowed uncertainty band may be responsible for changes in the typical energy of nonthermal photons.

$$E'_\gamma = \begin{cases} E'_{\gamma,\mathrm{th}} & \text{for } \tau'_T > 1 \\ E'_{\gamma,\mathrm{non\text{-}th}} & \text{for } \tau'_T \le 1. \end{cases} \quad (6)$$

Note that, although Eq. (6) defines characteristic photon energies, we include specific spectral shapes of the non-thermal and thermal photon energy spectra in the numerical computations as well as in the following discussion (including Fig. 2).

B. Proton acceleration and cooling processes

The acceleration time (acc) of a proton with comoving energy E'_p is

$$t'_{\mathrm{acc}} = \frac{E'_p}{B' ec} \simeq 3.7\times 10^{-9}\ \mathrm{s}\frac{E'_{p,\mathrm{GeV}}\theta_{j,7}t_{v,-2}\Gamma^3_{b,2.5}t^{1/2}_{j,1}}{\epsilon^{1/2}_{B,-1}E^{1/2}_{j,51}(1+z)^2}, \quad (7)$$

under the assumption of perfectly efficient acceleration. In the presence of a magnetic field, protons are subject to synchrotron cooling (sync) besides being accelerated:

$$t'_{\mathrm{sync}} = \frac{3m_p^4c^3 8\pi}{4\sigma_T m_e^2 E'_p B'^2} \simeq 5\times 10^9\ \mathrm{s}\frac{\theta^2_{j,7}t_{j,1}\Gamma^6_{b,2.5}t_{v,-2}E^{-1}_{j,51}}{E'_{p,\mathrm{GeV}}\epsilon_{B,-1}(1+z)^4}. \quad (8)$$

The inverse Compton process (IC) is another cooling channel. We express it as a function of E'_p for the Thomson and Klein-Nishina regimes [48],

$$t'_{\mathrm{IC}} = \begin{cases} \frac{3m_p^4c^3}{4\sigma_T m_e^2 E'_p E'_\gamma n'_\gamma} \simeq 5\times 10^9\mathrm{s}\frac{\theta^2_{j,7}t_{j,1}\Gamma^6_b t^2_{v,-2}E^{-1}_{j,51}}{E'_{p,\mathrm{GeV}}\epsilon_{e,-1}(1+z)^4}, \\ \frac{3E'_pE'_\gamma}{4\sigma_T m_e^2 c^5 n'_\gamma} \simeq 6\times 10^3\mathrm{s}\frac{E'_{p,\mathrm{GeV}}E'^2_{\gamma\mathrm{MeV}}\theta^2_{j,7}\Gamma^6_{b,2.5}t^2_{v,-2}}{E_{j,51}\epsilon_{e,-1}(1+z)^4 t^{-1}_{j,-1}}, \end{cases} \quad (9)$$

respectively, for $E'_p \ll (\gg) m_p^2c^4/E'_\gamma$, and with the comoving photon density

$$n'_\gamma = \frac{2E'_j\epsilon_e(1+z)}{\pi\theta_j^2\tilde{r}_j^2 ct_j\Gamma_b E'_\gamma}. \quad (10)$$

Because of the high density of photons, e^+e^- pairs may be produced through the Bethe-Heitler (BH) process: $p\gamma \to pe^+e^-$. The BH cross section is defined as in, e.g., Ref. [52],

$$\sigma_{\mathrm{BH}} = \alpha r_e^2\left\{\frac{28}{9}\ln\left[\frac{2E'_pE'_\gamma}{m_pm_ec^4}\right] - \frac{106}{9}\right\}, \quad (11)$$

with α the fine-structure constant and r_e the classical electron radius; the corresponding comoving cooling time is [48]

$$t'_{\mathrm{BH}} = \frac{E'_p(m_p^2c^4 + 2E'_pE'_\gamma)^{1/2}}{2n'_\gamma\sigma_{\mathrm{BH}}m_ec^3(E'_p+E'_\gamma)}. \quad (12)$$

The characteristic times of $p\gamma$ and pp interactions can be of relevance for the proton cooling, besides producing high-energy neutrinos as we will see in the next section. These are

$$t'_{p\gamma} = \frac{E'_p}{c\sigma_{p\gamma}n'_\gamma\Delta E'_p} \simeq 1.5\times 10^4\ \mathrm{s}\frac{\theta^2_{j,7}\Gamma^6_{b,2.5}t^2_{v,-2}t_{j,1}E'_{\gamma,\mathrm{MeV}}}{E_{j,51}\epsilon_{e,-1}(1+z)^4}, \quad (13)$$

$$t'_{pp} = \frac{E'_p}{c\sigma_{pp}n'_p\Delta E'_p} \simeq 1.4\times 10^4\ \mathrm{s}\frac{\Gamma^6_{b,2.5}\theta^2_{j,7}t^2_{v,-2}t_{j,1}}{E_{j,51}(1+z)^4}, \quad (14)$$

with cross sections $\sigma_{p\gamma} \simeq 5\times 10^{-28}\ \mathrm{cm}^{-2}$ and $\sigma_{pp} \simeq 5\times 10^{-26}\ \mathrm{cm}^{-2}$, respectively, and $\Delta E'_p/E'_p = 0.2(0.8)$ for $p\gamma$ (pp) interactions [48]. In the above equations, we neglect the integral over the energy range of the cross sections as well as the multipion production for sake of simplicity. Such approximations are not crucial given the purpose of our study, but we refer the interested reader to Refs. [14,53,54] for a discussion on the role of these factors on the total expected neutrino flux. Note that the expression for $t'_{p\gamma}$ is valid for E'_p above the threshold energy of the Δ resonance due to $p\gamma$ interactions ($E'_{p,\mathrm{th}} = [(m_\Delta c^2)^2 - (m_pc^2)^2]/4E'_\gamma$) [38,55].

Finally, protons are subject to the adiabatic cooling (ac), the time scale in the comoving frame of which is given by

$$t'_{\mathrm{ac}} = \frac{\tilde{r}_j}{\Gamma_b c} \simeq 6.3\ \mathrm{s}\Gamma_{b,2.5}t_{v,-2}(1+z)^{-1}. \quad (15)$$

The total cooling time of protons in the comoving frame is given by the superposition of the cooling processes mentioned above:

$$t'^{-1}_{c,p} = t'^{-1}_{\mathrm{syn}} + t'^{-1}_{\mathrm{IC}} + t'^{-1}_{\mathrm{BH}} + t'^{-1}_{p\gamma} + t'^{-1}_{pp} + t'^{-1}_{\mathrm{ac}}. \quad (16)$$

The maximum proton energy ($E_{p,\max}$) is determined by

$$t'_{c,p} = t'_{\mathrm{acc}}, \quad (17)$$

while the minimum proton energy ($E_{p,\min}$) is given by the proton rest mass.

To provide an idea of the relevant cooling processes for protons for both high and low Γ_b's, Fig. 1 shows (the inverse of) the proton cooling time scales as functions of the comoving proton energy for $\Gamma_b = 300$ (top panel) and $\Gamma_b = 3$ (bottom) jets at $z = 1$. In the high-Γ_b case, the maximum proton energy is $E'_{p,\max} = 1.5\times 10^9$ GeV, and it is determined by the competition of the shock acceleration with synchrotron cooling characterized by t'_{sync}. The

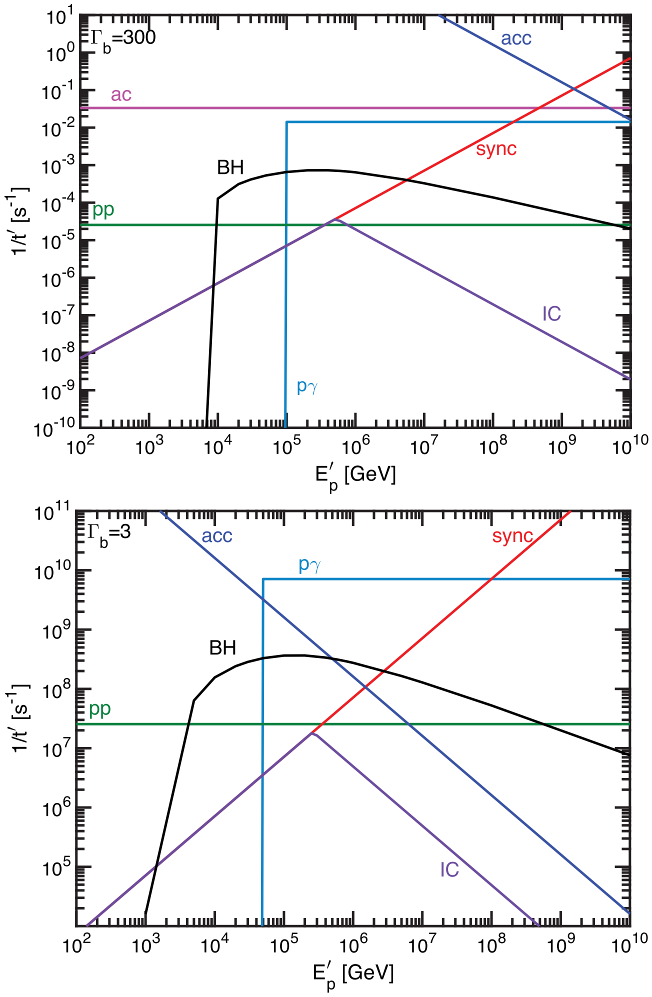

FIG. 1. Comoving cooling times for photomeson ($1/t'_{p\gamma}$ in light blue), proton-proton ($1/t'_{pp}$ in green), synchrotron radiation ($1/t'_{\rm syn}$ in red), inverse Compton ($1/t'_{\rm IC}$ in violet), BH ($1/t'_{\rm BH}$ in black), and adiabatic cooling ($1/t'_{\rm ac}$ in magenta) as functions of the comoving proton energy E'_p. The shock acceleration time ($1/t'_{\rm acc}$) is plotted in blue for comparison. The top (bottom) panel shows a typical jet with $\Gamma_b = 300$ ($\Gamma_b = 3$) at $z = 1$. The maximum proton energy is determined by $t'_{\rm syn}$ for $\Gamma_b = 300$ and by $t'_{p\gamma}$ for $\Gamma_b = 3$. Note that the adiabatic cooling time is below the minimum y-axis value in the $\Gamma_b = 3$ plot.

adiabatic cooling becomes instead the dominant cooling process for Γ_b higher than the one shown here. The low-Γ_b case has a maximum proton energy $E'_{p,\rm max} = 9.5 \times 10^4$ GeV fixed by the photomeson cooling ($t'_{p\gamma}$). Note that pp interactions occur for the whole proton energy range independently from Γ_b, while $p\gamma$ interactions are relevant for E'_p larger than the threshold energy of the Δ resonance. However, as discussed in the next section, the energy range where $p\gamma$ interactions are relevant becomes smaller as Γ_b decreases, until $p\gamma$ interactions are negligible for low Γ_b and only pp interactions affect the neutrino spectrum (see the case shown in the bottom panel of Fig. 1).

C. Meson cooling processes and neutrino production

High-energy neutrinos are produced by the protons interacting with the synchrotron photons ($p\gamma$ interactions) and with the protons present in the shock region (pp interactions) [56,57]. Both interactions produce $\pi^\pm$ and $K^\pm$ that then decay to muons and neutrinos.

Pions and kaons are affected by hadronic cooling,

$$t'_{\rm hc} = \frac{E'_a}{\Delta E'_a c \sigma_h n'_p} = t'_{\rm pp}, \tag{18}$$

with $\Delta E'_\pi = 0.8 E'_\pi$ the energy lost by the incident meson in each collision (Figs. 18 and 19 in Ref. [58]) and $\sigma_h = 5 \times 10^{-26}$ cm^{-2} the cross section for meson-proton collisions [59]. Similarly to protons, pions, kaons, and muons are also subject to synchrotron and IC cooling [defined as in Eqs. (8) and (9) with $E'_p \to E'_a$ and $m_p \to m_a$, where $a = \pi$, K, and μ] as well as to adiabatic cooling [Eq. (15)].

The total cooling time of pions, kaons, and muons is

$$t'^{-1}_c = t'^{-1}_{\rm syn} + t'^{-1}_{\rm hc} + t'^{-1}_{\rm IC} + t'^{-1}_{\rm ac}. \tag{19}$$

(Note that muons are not subject to hadronic cooling.) As explained in the next section, by comparing the above cooling times with the lifetime of mesons and muons, one can predict the expected neutrino spectrum.

D. Neutrino energy spectrum

We assume an initial proton spectrum that scales as E'^{-2}_p. As for $p\gamma$ interactions, the comoving proton energy to produce a Δ resonance (and therefore to generate neutrinos) is $E'_p \geq [(m_\Delta c^2)^2 - (m_p c^2)^2]/(4E'_\gamma)$. This energy will affect the correspondent neutrino spectrum at

$$\begin{aligned} E_{\nu,b} &= a_i \left(\frac{\Gamma}{1+z}\right)^2 \frac{(m_\Delta c^2)^2 - (m_p c^2)^2}{4E_\gamma} \\ &\simeq 7.5 \times 10^5 \text{ GeV} \left(\frac{a_i}{0.05}\right) \frac{\Gamma^2_{b,2.5}}{(1+z)^2 E_{\gamma,\rm MeV}}, \end{aligned} \tag{20}$$

with E_γ the characteristic energy of the photon spectrum [Eq. (6)]. The numerical factor a_i is $a_\pi = 0.05$ (20% being the fraction of E_p that goes into pions and $1/4$ being the fraction of the E_π carried by neutrinos), $a_{\mu_\pi} = 0.05$ (as $3/4$ is the energy fraction transferred from pions to muons and $1/3$ takes into account the three-body decay of the muon), $a_K = 0.1$ (20% is the fraction of E_p that goes into E_K, and $1/2$ is the fraction of E_K carried by neutrinos), and $a_{\mu_K} = 0.033$ for muons originating from the kaon decay. Note that Eq. (20) defines a spectral break in the neutrino energy spectrum for $\tau_T \ll 1$, where the photon spectrum is a broken power law; it represents the threshold energy of the neutrino spectrum for the case with $\tau_T \gg 1$ (see Fig. 2).

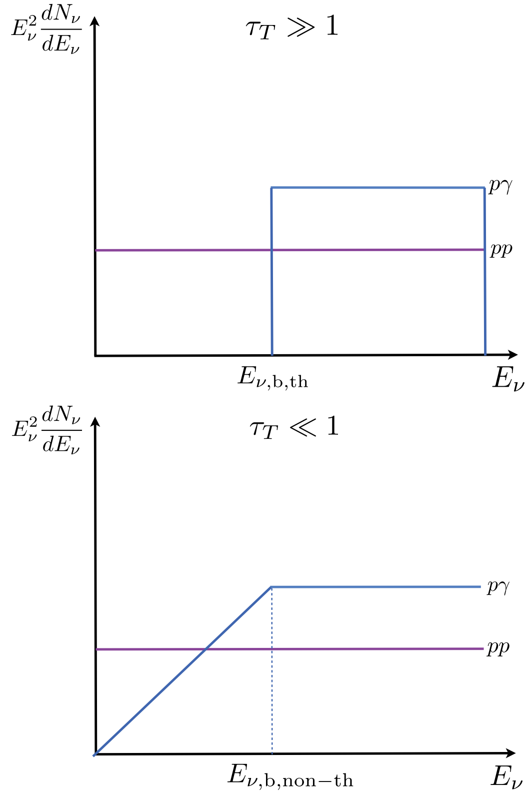

FIG. 2. Diagram for the neutrino energy spectrum in the absence of meson cooling effects. The top (bottom) panel refers to the $\tau_T \gg 1$ ($\tau_T \ll 1$) case. For each case, the spectra from pp and $p\gamma$ interactions are shown in arbitrary units. The relative normalization of the pp spectrum with respect to the $p\gamma$ one is also arbitrary.

The initial neutrino energy spectrum before being affected by meson cooling processes is sketched in Fig. 2 for $\tau_T \gg 1$ (top) and $\tau_T \ll 1$ (bottom). For $\tau_T \gg 1$, given the sharp drop of the blackbody energy spectrum (see Sec. II A), the neutrino spectrum can be approximated by a rectangular function different from zero for $E'_{\nu,b} < E'_\nu < E'_{\nu,\mathrm{max}}$. For $\tau_T \ll 1$, the neutrino spectrum will be the same as the proton spectrum above $E'_{\nu,b}$, while it will be harder at lower energies (see also the discussion in Refs. [38,55]).

Because of the cooling processes of pions, kaons, and muons described in Sec. II C, the neutrino spectrum is given by

$$\left(\frac{dN_\nu}{dE'_\nu}\right)_{\mathrm{inj}} = \left(\frac{dN_\nu}{dE'_\nu}\right)_0 \left[1 - \exp\left(-\frac{t'_{c,a} m_a}{E'_a \tau_a}\right)\right], \tag{21}$$

with $E'^2_\nu (dN_\nu/dE'_\nu)_0$ defined as in Fig. 2 according to the value of τ_T and τ_a as the lifetime of mesons or muons. The minimum and maximum energies of the neutrino spectrum are defined by the minimum and maximum proton energies introduced in Sec. II B.

The ν_e and ν_μ neutrino energy spectra produced from pion decay are

$$\left(\frac{dN_{\nu_e}}{dE'_\nu}\right)_{\mathrm{inj},\pi} = \left(\frac{dN_\nu}{dE'_\nu}\right)_{\mu_\pi}, \tag{22}$$

$$\left(\frac{dN_{\nu_\mu}}{dE'_\nu}\right)_{\mathrm{inj},\pi} = \left(\frac{dN_\nu}{dE'_\nu}\right)_{\mu_\pi} + \left(\frac{dN_\nu}{dE'_\nu}\right)_{\pi}. \tag{23}$$

Similar relations hold for neutrinos produced by kaon decay. No ν_τ's are produced at the source. However, neglecting nonstandard scenarios, the three neutrino flavors become similarly abundant after flavor oscillations on their way to Earth [25]. Flavor conversions in matter might also occur while neutrinos are propagating within the jet in optically thick sources (see, e.g, Refs. [60–64]). However, in the following, we will neglect flavor oscillations in matter as they would not affect our conclusions. Nonetheless, future constraints on the neutrino flavor ratio observed on Earth might provide us with indirect information on the progenitor structure of optically thick sources in the case of the successful observation of baryon-rich bursts.

By adapting the normalization proposed in Ref. [65], the observed neutrino spectrum for a single source at redshift z and for each neutrino production channel a is

$$F_\nu(E_\nu, z) = \frac{(1+z)^3}{2\pi\theta_j^2 \Gamma_b d_L^2} E'_j N_a f_p [1 - (1-\chi_p)^{\tau'_p}] \left(\frac{dN_\nu}{dE'_\nu}\right)_{\mathrm{inj}} \tag{24}$$

with $N_\pi = N_{\mu_\pi} = 0.12$, $N_K = 0.01$, $N_{\mu_K} = 0.003$ [38], and $\tau'_p = \tau'_{pp}(z, E'_\nu) + \tau'_{p\gamma}(z, E'_\nu) = \tilde{r}_j/\Gamma_b(\sigma_{p\gamma} n'_\gamma + \sigma_{pp} n'_p)$ [48], and $(dN_\nu/dE'_\nu)_{\mathrm{inj}}$ is the normalized spectrum that satisfies $\int dE'_\nu E'_\nu (dN_\nu/dE'_\nu)_{\mathrm{inj}} = 1$. The factor f_p takes into account the effect of spectral breaks,

$$f_p = \frac{\int_0^\infty dE'_\nu E'_\nu (\frac{dN_\nu}{dE'_\nu})_{\mathrm{inj}}}{\int_0^\infty dE'_\nu E'_\nu (\frac{dN_\nu}{dE'_\nu})_{\mathrm{inj,no\text{-}break}}}, \tag{25}$$

where $(dN_\nu/dE'_\nu)_{\mathrm{inj,no\text{-}break}} \propto E'^{-2}_\nu$ is the neutrino spectrum without any cooling breaks [Eq. (21)] as well as the break due to the threshold of $p\gamma$ interaction [Eq. (20)]; the denominator is therefore proportional to $\ln(E'_{p,\mathrm{max}}/E'_{p,\mathrm{min}})$. Finally, the neutrino energy in the jet frame is related to that in the observer frame through $E'_\nu = E_\nu(1+z)/\Gamma_b$, and $d_L(z)$ is the luminosity distance defined in a flat ΛCDM cosmology with $\Omega_m = 0.32$, $\Omega_\Lambda = 0.68$, and $H_0 = 67\ \mathrm{km\,s^{-1}\,Mpc^{-1}}$ for the Hubble constant [66].

Figure 3 shows the fluence of a burst at $z = 1$ as a function of Γ_b as from Eq. (24) and after flavor oscillations. For $\Gamma_b = 3$ and 30, the spectrum is clearly dominated by

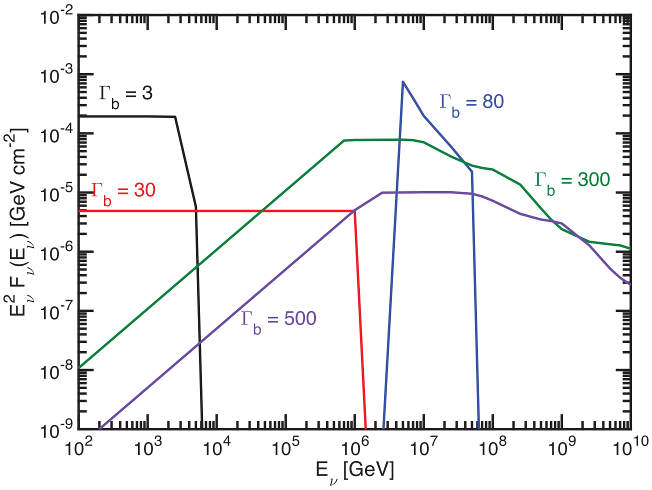

FIG. 3. Expected fluence for a single flavor of an astrophysical burst at $z = 1$ with $\Gamma_b = 3$ (black), 30 (red), 80 (blue), 300 (green), and 500 (violet). While pp interactions dominate for $\Gamma_b = 3$ and 30, $p\gamma$ interactions are responsible for shaping the neutrino spectrum in the case of $\Gamma_b = 300$ and 500. The case with $\Gamma_b = 80$ is an intermediate case where both pp and $p\gamma$ interactions are effective, although only the latter component is visible here.

pp interactions, while for $\Gamma_b = 300$ and 500, it is dominated by $p\gamma$ interactions. The spectrum at $\Gamma_b = 80$ is mainly determined by pp interactions at low energies (not visible in the plot because the flux is lower than the bottom value of the y axis of the plot) and by $p\gamma$ interactions in the region around 10^7 GeV. The sharp rise of the neutrino spectrum at about 10^7 GeV is due to the fact that this object is optically thick ($\tau_T > 1$) and the correspondent initial neutrino spectrum has a sharp rise due to the blackbody photon spectrum distribution (see Fig. 2).

III. DIFFUSE HIGH-ENERGY NEUTRINO EMISSION FROM ASTROPHYSICAL BURSTS

We assume that the redshift evolution of baryon-rich and ordinary high-luminosity GRBs is a function of the redshift and of the Lorentz boost factor; $R_j(z,\Gamma_b)d\Gamma_b = R(z)\xi(\Gamma_b)d\Gamma_b$ is the formation rate density of the bursts with the Lorentz factor between Γ_b and $\Gamma_b + d\Gamma_b$. The redshift-dependent part of $R_j(z,\Gamma_b)$ follows the star formation rate [67]

$$R(z) \propto \left[(1+z)^{p_1 k} + \left(\frac{1+z}{5000}\right)^{p_2 k} + \left(\frac{1+z}{9}\right)^{p_3 k}\right]^{1/k}, \tag{26}$$

with $k = -10$, $p_1 = 3.4$, $p_2 = -0.3$, and $p_3 = -3.5$, and is normalized such that $R(0) = 1$. As for the Γ_b dependence on the rate, we assume $\xi(\Gamma_b) = \Gamma_b^{\alpha_\Gamma}\beta_\Gamma$ and fix the parameters α_Γ and β_Γ in such a way that

$$\int_1^{10^3} d\Gamma_b \Gamma_b^{\alpha_\Gamma}\beta_\Gamma = R_{\rm SN}(0)\zeta_{\rm SN}\frac{\theta^2_{\rm SN}}{2}, \tag{27}$$

$$\int_{200}^{10^3} d\Gamma_b \Gamma_b^{\alpha_\Gamma}\beta_\Gamma = \rho_{0,\rm HL-GRB}, \tag{28}$$

where $\zeta_{\rm SN}$ is the fraction of core-collapse SNe that develop jets, $\theta^2_{\rm SN}/2$ is the fraction of the jet pointing toward us, $R_{\rm SN}(0) \simeq 2\times 10^5$ Gpc^{-3} yr^{-1} [68,69] is the local SN rate, and $\rho_{0,\rm HL-GRB} = 0.8$ Gpc^{-3} yr^{-1} is an optimistic estimation of the observed local high-luminosity GRB rate [70]. To give an idea of the dependence of $R_j(z,\Gamma_b)$ on Γ_b, Fig. 4 shows $R_j(z=0,\Gamma_b)$ as a function of Γ_b for fixed $\rho_{0,\rm HL-GRB}$ and $\zeta_{\rm SN} = 1$, 100%, respectively.

The total diffuse neutrino intensity from all bursts is therefore defined in the following way:

$$I(E_\nu) = \int_{\Gamma_{\rm b,min}}^{\Gamma_{\rm b,max}} d\Gamma_b \int_{z_{\rm min}}^{z_{\rm max}} dz \frac{c}{2\pi\theta_j^2 H_0\Gamma_b} \times \frac{1}{\sqrt{\Omega_M(1+z)^3+\Omega_\Lambda}} R_j(z,\Gamma_b)E'_j f_p N_a \times [1-(1-\chi_p)^{\tau'_p}]\left(\frac{dN_{\nu_\mu}}{dE'_\nu}\right)_{\rm osc}. \tag{29}$$

The top panel of Fig. 5 shows the total diffuse emission from astrophysical bursts as a function of the neutrino energy for one neutrino flavor obtained by assuming $[z_{\rm min}, z_{\rm max}] = [0,7]$ and $[\Gamma_{\rm b,min},\Gamma_{\rm b,max}] = [1,10^3]$. The continuous line stands for $\zeta_{\rm SN} = 10\%$, while the dashed (dot-dashed) line is obtained by adopting $\zeta_{\rm SN} = 100\%$ (1%). For comparison, the IceCube data as well as a band corresponding to the single power-law fit [21] are shown. The figure shows that these jets could represent a major component of the flux of the IceCube neutrinos for $\zeta_{\rm SN} < 10\%$, especially in the PeV energy range.

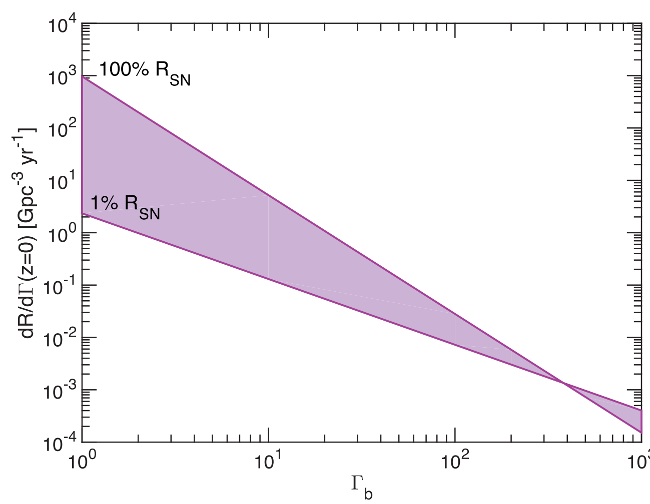

FIG. 4. Local formation rate of the jets per unit volume per unit Γ_b, $R_j(z=0,\Gamma_b)$, as a function of Γ_b for fixed $\rho_{0,\rm HL-GRB}$ and $\zeta_{\rm SN} = 1$, 100%, respectively (see the text for details).

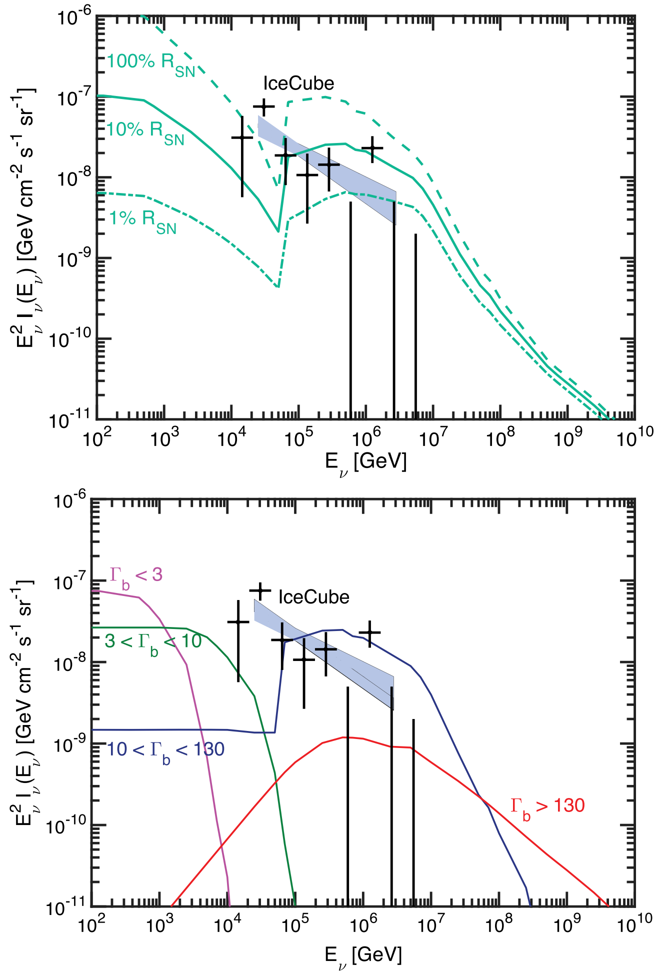

FIG. 5. Top panel: Diffuse intensity for one neutrino flavor after flavor oscillations as a function of the energy and for $\zeta_{\mathrm{SN}} = 1$, 10, and 100%, plotted with a dashed, solid, and dot-dashed lines, respectively. The blue band and the black data points correspond to the best-fit power-law model and the IceCube data from Ref. [21]. $\zeta_{\mathrm{SN}} = 100\%$ is incompatible with the current IceCube data, while $\zeta_{\mathrm{SN}} = 10\%$ is marginally allowed. Bottom panel: Partial contributions to the diffuse neutrino intensity for one neutrino flavor from different regimes of Γ_b, for $\zeta_{\mathrm{SN}} = 10\%$. As Γ_b increases, the neutrino spectrum peaks at larger neutrino energies.

Assuming that baryon-rich jets and ordinary GRBs all belong to the same family and evolve by following $R_j(z, \Gamma_b)$, one can also indirectly constrain the local rate of baryon-rich bursts by adopting the IceCube high-energy neutrino data. In fact, Fig. 5 suggests that a local rate of baryon-rich jets with ζ_{SN} higher than tens of percent is excluded from the current IceCube data set. Our findings on the abundance of baryon-rich jets are also in agreement with the ones in Ref. [71], where the local abundance of transient sources of high-energy neutrinos is found to be lower than 10 $\mathrm{Gpc}^{-3}\,\mathrm{yr}^{-1}$ so as not to contradict the non-observation of such sources in dedicated neutrino searches.

To disentangle the dependence of the neutrino diffuse intensity from Γ_b, the bottom panel of Fig. 5 shows partial contributions to the total diffuse emission from different regimes of Γ_b for $\zeta_{\mathrm{SN}} = 10\%$. As Γ_b increases, the neutrino intensity peaks at higher energies. The flux for $\Gamma_b > 130$ reproduces the expected diffuse intensity from high-luminosity GRBs in the PeV energy range; on the other hand, jets with $\Gamma_b < 10$ are responsible for a neutrino flux that is relevant in the TeV energy range (see also, e.g., Refs. [38,72] about the typical neutrino energy spectra from $p\gamma$ and pp interactions). For the assigned input parameters, astrophysical bursts with $10 < \Gamma_b < 130$ are responsible for a neutrino flux compatible with the current IceCube neutrino data set for particular values of ζ_{SN}. Such jets belong to an intermediate class between choked and high-luminosity GRBs, which is optically thick and in which pp and $p\gamma$ interactions are both relevant, as discussed in Sec. II D.

IV. UNCERTAINTIES OF THE JET MODEL PARAMETER

The results presented in Sec. III have been obtained by assuming a simple model with common properties for all GRBs, except for the Lorentz factor Γ_b. Our conclusions are, however, limited by the astrophysical uncertainties. For example, we assumed that the local rate of successful GRBs is given by $\rho_{0,\mathrm{HL-GRB}} = 0.8\ \mathrm{Gpc}^{-3}\,\mathrm{yr}^{-1}$ [70]; this is an optimistic assumption as the local rate could be as low as 0.5 $\mathrm{Gpc}^{-3}\,\mathrm{yr}^{-1}$ [70]. We also consider the simplest possible scaling law of the local cosmic rate of astrophysical jets as a function of Γ_b [Eq. (28)], given the lack of data; other possible scaling relations might describe better the real GRB family. We currently do not have data to describe the engine behind low-Γ_b jets and extrapolate their properties from the ones measured for successful jets. Future observations may help to reduce such uncertainties [1] that we currently expect might be responsible for a variation of up to 1 or 2 orders of magnitude of the estimated best-fit value of the flux.

Besides the local abundance of baryon-rich sources, the jet energy may also be a variable parameter. Figure 6 represents ζ_{SN} as a function of $\tilde{E}_j$. The contour plot shows the allowed abundance of baryon-rich bursts from the current IceCube high-energy neutrino data set [21]; the yellow region is compatible with the IceCube data, while the dark green one is excluded.[3] A region of marginally allowed $(\tilde{E}_j, \zeta_{\mathrm{SN}})$ falls in between (plotted in light green).

Although the high-energy neutrino flux detected by the IceCube telescope is in the same energy range where the

[3]We define the “allowed region” (“not-allowed region”) as the region of the parameter space where $[E_\nu^2 I_\nu(E_\nu)]_{\mathrm{theo}} \le [E_\nu^2 I_\nu(E_\nu)]_{\mathrm{IC,band}}$ ($[E_\nu^2 I_\nu(E_\nu)]_{\mathrm{theo}} > [E_\nu^2 I_\nu(E_\nu)]_{\mathrm{IC,band}}$) for all energy points E_ν of the IceCube data; the “marginally allowed region” is the transition region of the parameter space where roughly half of all energy points fall within one of the two previous categories.

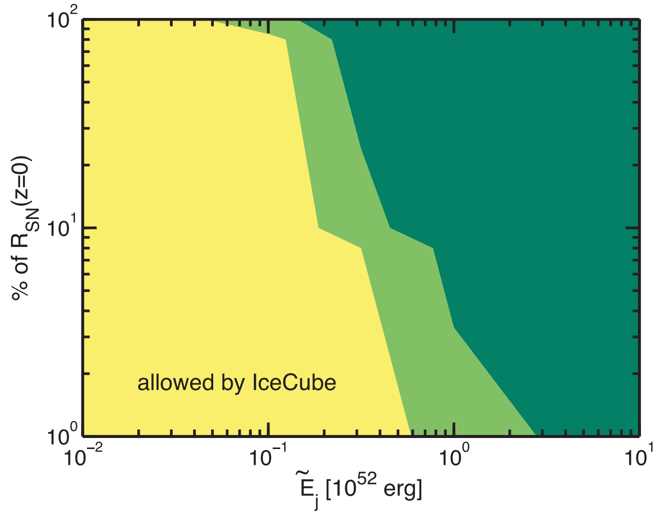

FIG. 6. Contour plot of the allowed abundance of choked bursts expressed as a fraction of the local supernova rate that forms choked jets, ζ_{SN}, and as a function of the jet energy $\tilde{E}_j$. The yellow region is compatible with the IceCube data [21], and the dark green one is excluded; the light green region is marginally compatible.

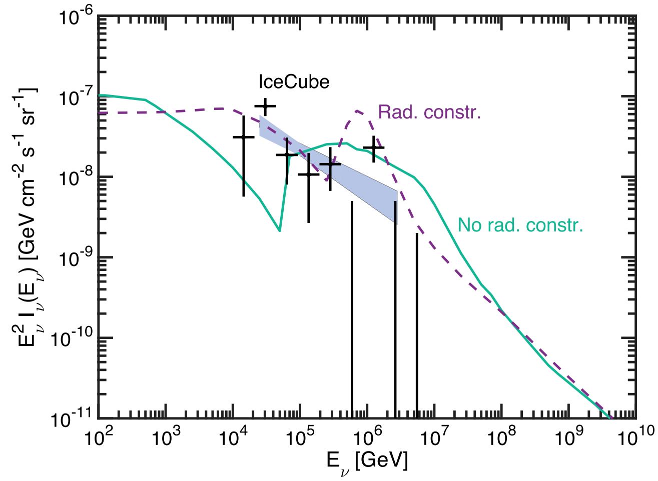

FIG. 7. Diffuse intensity for one neutrino flavor after flavor oscillations as a function of the energy and for $\zeta_{SN} = 10\%$. The blue band and the black data points correspond to the best-fit power-law model and the IceCube data from Ref. [21]. The green continuous line represents the total neutrino intensity of our standard jet model, and the violet dashed line is the total neutrino intensity when radiation constraints are taken into account (see the text for more details).

neutrino emission from intermediate-Γ_b jets peaks, we are able to provide bounds on the local rate of baryon-rich GRBs as a function of the jet energy by assuming a SN-GRB connection. Such constraints are roughly comparable with the ones presented in Ref. [12], obtained for choked sources. Note, however, that the bounds on $(\tilde{E}_j, \Gamma_b)$ in Ref. [12] were extrapolated on the basis of an analysis on point sources, and Γ_b was considered a fixed parameter typical of choked GRBs. Under the assumption of the SN-GRB connection, we expect that upper limits on the abundance of choked sources are going to become more stringent in the near future in light of the increasing statistics of the IceCube data sets.

We have assumed in this work that the parameters of each GRB are fixed during its duration. However, by including multiple internal shocks and assuming a non-narrow distribution in Γ_b in each GRB as, e.g., in the simulations presented in Ref. [73], a qualitatively similar phenomenology to the one described above might be of relevance also in the transition from optically thick to optically thin emission regions.

Thus far, we assumed that the burst duration is independent of Γ_b. If high-energy particles are emitted mainly through internal shocks, the internal collisions occurring between the plasma shells inside the jet could, however, spread out in time and yield burst durations longer than the assumed $\tilde{t}_j = 10$ s for bursts with low Γ_b. Although the dependence of t_j on Γ_b is relevant to describe the physics of astrophysical bursts, our assumption $[t_j(\Gamma_b) = \text{const.}]$ does not affect our conclusions; see the discussion about results presented in Fig. 7.

We work under the assumption that internal collisionless shocks are able to accelerate protons efficiently for any Lorentz factor Γ_b. As discussed in Refs. [37,74–76], this might not be the case if radiation-mediated shocks occur in choked sources; as a consequence, proton acceleration could not be as efficient as considered here, and the correspondent neutrino energy fluxes from baryon-rich sources might be affected. However, as shown in Fig. 5, the upper bound on ζ_{SN} should not be affected, since it is only indirectly constrained from the IceCube data from jets with intermediate Γ_b that should, at least partially, evade the radiation-dominated regime. To prove that, we include the condition to avoid radiation-mediated shocks for our representative case with $\xi_{SN} = 0.1$, following the discussion in Ref. [37]. We vary the burst duration as a function of Γ_b in such a way to recover the conservative bound: $\tau_T \leq 1$ [see Eq. (1)] for any redshift z. Specifically, we consider $t_j = 10$ s for $130 < \Gamma_b \leq 10^3$, $t_j = 500$ s for $50 < \Gamma_b \leq 130$, and $t_j = 10^6$ s for $\Gamma_b \leq 50$. Note that such a choice of t_j is also responsible for lower jet luminosities as Γ_b decreases in agreement with the upper bounds on the luminosity shown in Fig. 3 of Ref. [37] in order to evade the radiation-dominated regime. The total neutrino intensity computed within this setup is plotted in Fig. 7 (dashed violet curve), and it should be compared with the continuous green curve representing the total diffuse intensity for constant $t_j = 10$ s also shown in the top panel of Fig. 5. The condition $\tau_T \leq 1$ affects the leading cooling processes discussed in Sec. II B as a function of Γ_b and the final shape of the expected neutrino intensity as shown in Fig. 7, but it does not drastically modify our conclusions.

Reference [77] pointed out that the collimation shock in the jet inside the star might be of relevance for the jet dynamics and, as discussed in Ref. [37], it might also affect the neutrino production. On the basis of the study presented here, we conclude that our main results are robust even with respect to the inclusion of such an effect now discarded. Nevertheless, further modeling of the jet properties by adding all the factors mentioned above is required, especially in light of the fact that jets with intermediate values of Γ_b could produce a neutrino diffuse flux comparable to the one detected from IceCube.

V. CONCLUSIONS

The most likely scenario explaining the formation of the long-duration astrophysical bursts is the development of a jet out of a black hole or an accretion disk, soon after the core collapse of a supernova. However, observational evidence suggests that only a small fraction of supernovae evolves into high-luminosity gamma-ray bursts with highly relativistic jets. Probably, softer jets, invisible or scarcely visible electromagnetically, could originate from the remaining optically thick supernova heirs. These objects are possibly even more abundant that the ones leading to visible GRBs and have been dubbed baryon-rich jets in this work.

In this paper, we study the SN-GRB connection, by assuming that ordinary high-luminosity GRBs and baryon-rich jets originate from the same class of sources having core-collapse supernovae as common progenitors. We hypothesize that the local rate of such sources decreases as the Lorentz boost factor Γ_b increases. To investigate the neutrino emission from this class of astrophysical jets, we define a general neutrino emission model, including hadronuclear and photomeson interactions as well as cooling processes for mesons and protons. For simplicity, we assume that ordinary GRBs and baryon-rich jets have identical jet properties except for the Lorenz factor Γ_b, although we prove that our conclusions should not drastically change with respect to variations of the other model parameters.

We find that the neutrino fluence peaks in different energy ranges according to the Lorenz boost factor, ranging from TeV energies for low-Γ_b bursts to PeV energies for high-Γ_b bursts. The neutrino production in low-Γ_b jets is mainly due to hadronuclear interactions, while it is mainly determined by photon-meson interactions for bursts with high Γ_b.

The high-energy neutrino flux currently observed by the IceCube telescope could be generated, especially in the PeV region, from bursts with intermediate values of Γ_b with respect to the typical ones of baryon-rich and bright GRBs: $\Gamma_b \in [10, 130]$. Such sources with intermediate values of Γ_b are optically thick, therefore not or scarcely visible in photons, and pp and $p\gamma$ interactions are both effective for what concerns the neutrino production.

Under the assumption that supernovae evolve in astrophysical bursts with variable Γ_b, we point out that by comparing the diffuse emission of high-energy neutrinos from jets with intermediate values of Γ_b with the current best fit of the IceCube high-energy neutrino flux one could put indirect constraints on the local rate of choked GRBs. We find that the present IceCube data sets favor a local rate of choked sources lower than tens of percent of the local core-collapse supernova rate. Such constraints are roughly compatible with upper limits coming from dedicated searches on choked sources from the IceCube Collaboration. However, we expect them to become tighter in the near future in light of the increasing IceCube statistics and future generation neutrino telescopes [78].

ACKNOWLEDGMENTS

We thank Imre Bartos, Mauricio Bustamante, Kohta Murase, and Walter Winter for comments on the manuscript. This work was supported by Netherlands Organization for Scientific Research through a Vidi grant.

[1] P. Mészáros, arXiv:1511.01396.
[2] P. Kumar and B. Zhang, Phys. Rep. **561**, 1 (2014).
[3] P. Mészáros, Rep. Prog. Phys. **69**, 2259 (2006).
[4] E. Waxman, Phys. Rev. Lett. **75**, 386 (1995).
[5] M. Vietri, Astrophys. J. **453**, 883 (1995).
[6] S. E. Woosley and J. S. Bloom, Annu. Rev. Astron. Astrophys. **44**, 507 (2006).
[7] S. E. Woosley, Astrophys. J. **405**, 273 (1993).
[8] R. Abbasi *et al.* (IceCube Collaboration), Astrophys. J. **710**, 346 (2010).
[9] R. Abbasi *et al.* (IceCube Collaboration), Phys. Rev. Lett. **106**, 141101 (2011).
[10] R. Abbasi *et al.* (IceCube Collaboration), Nature (London) **484**, 351 (2012).
[11] M. G. Aartsen *et al.* (IceCube Collaboration), Astrophys. J. **805**, L5 (2015).
[12] R. Abbasi *et al.* (IceCube and ROTSE Collaborations), Astron. Astrophys. **539**, A60 (2012).
[13] M. G. Aartsen *et al.*, Astrophys. J. **816**, 75 (2016).
[14] P. Baerwald, S. Hümmer, and W. Winter, Astropart. Phys. **35**, 508 (2012).
[15] H. N. He, R. Y. Liu, X. Y. Wang, S. Nagataki, K. Murase, and Z. G. Dai, Astrophys. J. **752**, 29 (2012).

[16] I. Bartos, A. M. Beloborodov, K. Hurley, and S. Márka, Phys. Rev. Lett. **110**, 24 (2013).
[17] M. G. Aartsen *et al.* (IceCube Collaboration), Science **342**, 1242856 (2013).
[18] M. G. Aartsen *et al.* (IceCube Collaboration), Phys. Rev. Lett. **111**, 021103 (2013).
[19] M. G. Aartsen *et al.* (IceCube Collaboration), Phys. Rev. Lett. **113**, 101101 (2014).
[20] M. G. Aartsen *et al.* (IceCube Collaboration), Phys. Rev. D **91**, 022001 (2015).
[21] M. G. Aartsen *et al.* (IceCube Collaboration), Astrophys. J. **809**, 98 (2015).
[22] M. G. Aartsen *et al.* (IceCube Collaboration), Phys. Rev. Lett. **115**, 081102 (2015).
[23] E. Waxman, arXiv:1511.00815.
[24] K. Murase, arXiv:1511.01590.
[25] L. A. Anchordoqui *et al.*, JHEAp **1–2**, 1 (2014).
[26] I. Tamborra, S. Ando, and K. Murase, J. Cosmol. Astropart. Phys. 09 (2014) 043.
[27] S. Ando, I. Tamborra, and F. Zandanel, Phys. Rev. Lett. **115**, 221101 (2015).
[28] K. Bechtol, M. Ahlers, M. Di Mauro, M. Ajello, and J. Vandenbroucke, arXiv:1511.00688.
[29] T. Glüsenkamp (IceCube Collaboration), arXiv:1502.03104.
[30] K. Murase, D. Guetta, and M. Ahlers, Phys. Rev. Lett. **116**, 071101 (2016).
[31] M. D. Kistler, arXiv:1511.01530.
[32] E. Waxman and J. N. Bahcall, Phys. Rev. D **59**, 023002 (1998).
[33] K. Murase, K. Ioka, S. Nagataki, and T. Nakamura, Astrophys. J. **651**, L5 (2006).
[34] N. Gupta and B. Zhang, Astropart. Phys. **27**, 386 (2007).
[35] R. Y. Liu, X. Y. Wang, and Z. G. Dai, Mon. Not. R. Astron. Soc. **418**, 1382 (2011).
[36] R. Y. Liu and X. Y. Wang, Astrophys. J. **766**, 73 (2013).
[37] K. Murase and K. Ioka, Phys. Rev. Lett. **111**, 121102 (2013).
[38] I. Tamborra and S. Ando, J. Cosmol. Astropart. Phys. 09 (2015) 036.
[39] N. Fraija, JHEAp **9–10**, 25 (2015).
[40] E. Nakar, Astrophys. J. **807**, 172 (2015).
[41] I. Bartos, B. Dasgupta, and S. Márka, Phys. Rev. D **86**, 083007 (2012).
[42] D. Guetta and M. Della Valle, Astrophys. J. **657**, L73 (2007).
[43] A. MacFadyen and S. E. Woosley, Astrophys. J. **524**, 262 (1999).
[44] B. Paczynski, Astrophys. J. **494**, L45 (1998).
[45] P. Mészáros and E. Waxman, Phys. Rev. Lett. **87**, 171102 (2001).
[46] S. Razzaque, P. Mészáros, and E. Waxman, Phys. Rev. D **68**, 083001 (2003).
[47] S. Ando and J. F. Beacom, Phys. Rev. Lett. **95**, 061103 (2005).
[48] S. Razzaque, P. Mészáros, and E. Waxman, Mod. Phys. Lett. A **20**, 2351 (2005).
[49] S. Horiuchi and S. Ando, Phys. Rev. D **77**, 063007 (2008).
[50] J. Kakuwa, K. Murase, K. Toma, S. Inoue, R. Yamazaki, and K. Ioka, Mon. Not. R. Astron. Soc. **425**, 514 (2012).
[51] E. Waxman, Lect. Notes Phys. **598**, 393 (2003).
[52] S. Razzaque, P. Mészáros, and E. Waxman, Phys. Rev. Lett. **93**, 181101 (2004) **94**, 109903(E) (2005).
[53] K. Murase and S. Nagataki, Phys. Rev. Lett. **97**, 051101 (2006).
[54] P. Baerwald, S. Hümmer, and W. Winter, Phys. Rev. D **83**, 067303 (2011).
[55] D. Guetta, D. Hooper, J. Alvarez-Muniz, F. Halzen, and E. Reuveni, Astropart. Phys. **20**, 429 (2004).
[56] S. R. Kelner, F. A. Aharonian, and V. V. Bugayov, Phys. Rev. D **74**, 034018 (2006) **79**, 039901(E) (2009).
[57] S. R. Kelner and F. A. Aharonian, Phys. Rev. D **78**, 034013 (2008) **82**, 099901(E) (2010).
[58] A. E. Brenner *et al.*, Phys. Rev. D **26**, 1497 (1982).
[59] S. Eidelman *et al.* (Particle Data Group Collaboration), Phys. Lett. B **592**, 1 (2004).
[60] T. Kashti and E. Waxman, Phys. Rev. Lett. **95**, 181101 (2005).
[61] O. Mena, I. Mocioiu, and S. Razzaque, Phys. Rev. D **75**, 063003 (2007).
[62] N. Fraija, Mon. Not. R. Astron. Soc. **437**, 2187 (2014).
[63] D. Xiao and Z. G. Dai, Astrophys. J. **805**, 137 (2015).
[64] N. Fraija, Mon. Not. R. Astron. Soc. **450**, 2784 (2015).
[65] S. Hümmer, P. Baerwald, and W. Winter, Phys. Rev. Lett. **108**, 231101 (2012).
[66] P. A. R. Ade *et al.* (Planck Collaboration), Astron. Astrophys. **571**, A16 (2014).
[67] H. Yuksel, M. D. Kistler, J. F. Beacom, and A. M. Hopkins, Astrophys. J. **683**, L5 (2008).
[68] T. Dahlen *et al.*, Astrophys. J. **613**, 189 (2004).
[69] L.-G. Strolger, T. Dahlen, S. A. Rodney, Or Graur, A. G. Riess, C. McCully, S. Ravindranath, B. Mobasher, and A. K. Shahady, Astrophys. J. **813**, 93 (2015).
[70] D. Wanderman and T. Piran, Mon. Not. R. Astron. Soc. **406**, 1944 (2010).
[71] M. Kowalski, J. Phys. Conf. Ser. **632**, 012039 (2015).
[72] K. Murase, Phys. Rev. D **78**, 101302 (2008).
[73] M. Bustamante, P. Baerwald, K. Murase, and W. Winter, Nat. Commun. **6**, 6783 (2015).
[74] A. Levinson and O. Bromberg, Phys. Rev. Lett. **100**, 131101 (2008).
[75] R. Budnik, B. Katz, A. Sagiv, and E. Waxman, Astrophys. J. **725**, 63 (2010).
[76] K. Murase, K. Kashiyama, and P. Mészáros, Phys. Rev. Lett. **111**, 131101 (2013).
[77] O. Bromberg, E. Nakar, T. Piran, and R. Sari, Astrophys. J. **740**, 100 (2011).
[78] M. G. Aartsen *et al.* (IceCube Collaboration), arXiv:1412.5106.